Physica B 610 (2021) 412858

Contents lists available at ScienceDirect

Physica B: Physics of Condensed Matter

journal homepage: http://www.elsevier.com/locate/physb

Study of structural, elastic, electronic, dynamical and optical properties of beryllium selenide (BeSe) semiconductor in zinc blend and NiAs phases

Mohamed Amine Ghebouli [a,b,*], Brahim Ghebouli [c,*], Tayeb Chihi [b], Messaoud Fatmi [b]

[a] Department of Chemistry, Faculty of Technology, University of Mohamed Boudiaf, M'sila, 28000, Algeria
[b] Research Unit on Emerging Materials (RUEM), University of Setif 1, 19000, Algeria
[c] Laboratory of Studies Surfaces and Interfaces of Solids Materials, Department of Physics, Faculty of Science, University Ferhat Abbas of Setif 1, 19000, Algeria

ARTICLE INFO

Keywords:
BeSe
Zinc blend
NiAs
Band structure
Band gap
Absorption

ABSTRACT

We report structural, elastic, electronic, dynamical and optical properties of beryllium selenide in zinc blend and NiAs phases. The zinc blend structure is the most stable at room temperature and equilibrium hydrostatic pressure. The HSE hybrid functional underestimates the lattice parameters compared to the GGA-PBE and LDA, but gives a fundamental gap closer to its experiment value. We derive bulk modulus, shear modulus, Young's modulus and Poisson's ratio using Voigt, Reuss and Hill approximations. Computed elastic constants in NiAs structure are predictions. Waves velocities for beryllium selenide in zinc blend (NiAs) phase along [100], [110] ([100], [110], [111]) directions are predictions. The indirect band gap Γ-X (2.852 eV) and Γ-K (0.536 eV) for BeSe in zinc blend and NiAs structures translates the semiconductor nature. Hybridization occurs between Se: p and Be: s states at the top of the valence band and traduces the covalent bonding character. The first conduction band is quite wide in both structures, where the contribution is due to Se: p, Se: s and Be: s sites. The electronic transition occurs from Se: p orbital of valence band to Be: s site of conduction band. Absorption peaks are attributed to the photo transition energies from the maximum valence band to the minimum conduction band under ultra violet light irradiation.

1. Introduction

Researchers are interested in studying binary II-VI semiconductors because of their technological applications. Beryllium selenide is semiconductor, where all properties depend on structure, pressure and temperature. The beryllium selenide takes the zinc blend structure at ambient temperature and equilibrium pressure. In this work, different functional such as GGA-PBE, LDA and HSE hybrid were used to obtain adequate structural, electronic and optical properties. The HSE hybrid functional underestimates the lattice parameters compared to the GGA-PBE and LDA, but gives a fundamental gap closer to its experiment value. Elastic constants for BeSe compound in NiAs phase are studied for the first time. Phonons dispersions curves for BeSe in zinc blend structure at various symmetry points show that optical (acoustical) phonons exhibit two couplets of longitudinal optical (LO) {longitudinal acoustical (LA)} and transverse optical (TO) {transverse acoustical (TA)} modes and confirm the dynamical stability of BeSe in zinc blend phase. The reflectivity in the ultra violet light domain (120–400 nm) is 63% (56%) in zinc blend (NiAs) structure. While in the visible light (400–800 nm), it is 43% (23%) for zinc blend (NiAs) phase. We detailed in this work structural, elastic, electronic, dynamical and optical properties for BeSe semiconductor in zinc blend and NiAs phases. We used the plane wave pseudo-potential method of density functional theory (DFT) within the generalized gradient approximation (GGA), the local density approximation (LDA) and HSE hybrid functional. For works carried out by other researchers on BeSe, it is quoted that the pressure induces a transition from zinc blend phase to NiAs structure for beryllium selenide at 56 GPa [1]. González-Díaz et al. studied elastic constants and electronic structure for BeSe in zinc blend phase using the local density approximation [2]. An experimental study on the electronic structure for beryllium selenide in zinc blend phase conducted by W. Yim et al. gave a band gap located between 4 and 4.5 eV [3]. Srivastava et al. studied structural parameters for BeSe in zinc blend phase by employing the plane-wave pseudo-potential method within the density functional theory [4]. R. Khenata et al. studied BeSe in zinc blend structure where they conclude that it is characterized by a small ionic radius ratio and a high degree of covalent bonding [5]. The investigation of B. Bouhafs et al. on the electronic structure and structural parameters for BeSe in

* Corresponding authors.
E-mail addresses: mohamedamine.ghebouli@univ-msila.dz (M. Amine Ghebouli), bghebouli@yahoo.fr (B. Ghebouli).

https://doi.org/10.1016/j.physb.2021.412858
Received 7 October 2020; Received in revised form 13 January 2021; Accepted 18 January 2021
Available online 25 February 2021

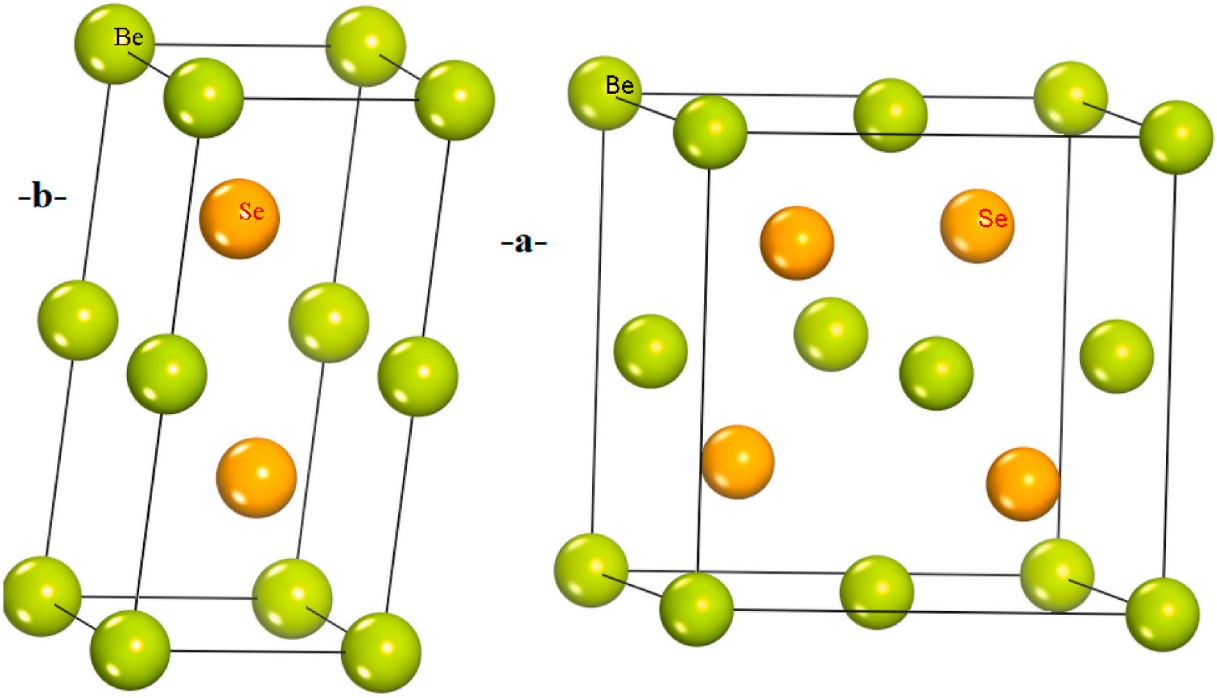

Fig. 1. Zinc blend (a) and NiAs (b) structures for BeSe.

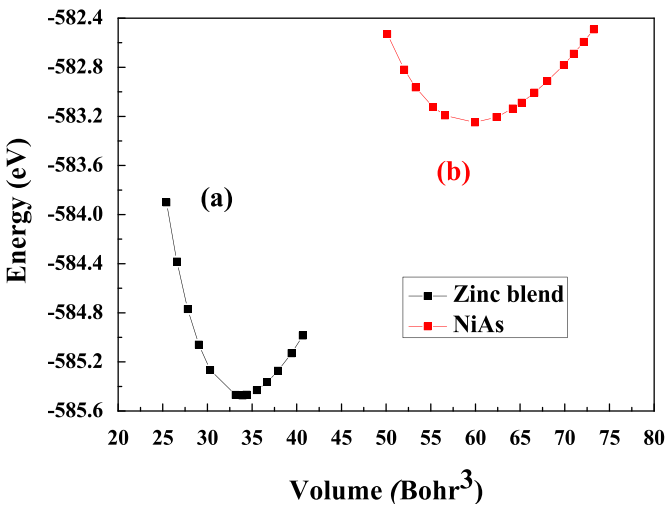

Fig. 2. Plots of total energy versus unit cell volume in zinc blend (a) and NiAs (b) structures for BeSe.

zinc blend phase presents a large band gap (2.7–5.5 eV) and high bulk modulus, which increased its hardness and stability [6]. Appropriate electronic and optical properties for BeSe make it technologically important material for applications in the area of catalysis to microelectronics and luminescent devices [7–9].

The organization of the paper is as follows: We explain the computational method in section 2. The results are presented and discussed in section 3. We conclude this work in section 4.

2. Computational method

First-principles calculations are performed using Cambridge Serial Total Energy Package (CASTEP) code [10]. Kohn–Sham equations are solved within the frame-work of density functional theory [11,12]. The interaction of valence electrons with ions cores is represented by the pseudo potential ultra soft non local Vanderbilt-type [13]. The energy E_{cut} of 660 eV and k-points of 8 × 8 × 8 using Monkhorst–Pack scheme [14] ensure well convergence of computed structure and energy. The computation of optical properties requires the use of 20 × 20 × 20 k-points. The exchange–correlation potential was treated within GGA, developed by Perdew, Burke and Ernzerhof [15], local density approximation (LDA) with Teter and Pade parameterization [16] and HSE hybrid functional. Structural parameters were determined using the Broyden–Fletcher–Goldfarb–Shanno (BFGS) minimization technique [17]. The tolerance for geometry optimization was set as the difference of total energy 5 × 10^{-6} eV/atom, maximum ionic Hellmann-Feynman force 0.01 eV/Å and maximum stress 0.02 eV/Å^3.

3. Results and discussions

3.1. Ground state properties

The electronic configuration of Be and Se atoms is Be:[He] $2s^2$ and Se:[Ar] $3d^{10}4s^24p^4$. The position of Be atom is located at the corner (0, 0, 0) in both phases. The Se atom takes place at (1/4, 1/4, 1/4) and (1/3, 2/3, 1/4) for zinc blend and NiAs phases respectively. Fig. 1 shows zinc blend and NiAs structures for BeSe. The study of structural characteristics requires the representation of total energy as a function of the volume of the elemental cell. Plots of total energy versus unit cell volume for BeSe in both phases are given in Fig. 2. The zinc blend phase is reported to be more stable than NiAs at room temperature and equilibrium pressure. This result is consistent with experimental and other theoretical works. Lattice parameters, bulk modulus and its pressure derivative for BeSe calculated with GGA, LDA and HSE hybrid approaches are listed in Table 1. Our results agree well with available experiment measurements [18] and theoretical data [4,19–28]. The lattice constant in zinc blend phase is closer to the experiment with a deviation of 0.1%. The HSE hybrid functional underestimates the lattice parameters compared with GGA-PBE and LDA in zinc blend and NiAs phases. Fig. 3 visualizes the dependence of formation enthalpy on pressure for beryllium selenide in zinc blend and NiAs phases by using GGA approach. We note that the two enthalpy-pressure diagrams have a similar behavior and show a transition region around 55 GPa. This value

Table 1
Lattice parameters, bulk modulus and its pressure derivative for BeSe in zinc blend and NiAs structures within GGA-PBE, LDA and HSE hybrid functional.

	Zinc blend GGA	LDA	HSE hybrid	Exp	other	NiAs GGA	LDA	HSE hybrid	Exp	other
a (Å)	5.129	5.083	4.976	5.139 [18]	5.137 [19] 5.037 [20] 5.087 [22]	3.513	3.456	3.415	3.524 [19] 3.421 [20] 3.502 [23]	
c (Å)						5.459	5.461	5.347	5.462 [19] 5.398 [20] 5.529 [23]	
B_0 (GPa)	74.50	87.35	99.484	92.20 [18]	74.97 [21] 80 [4] 96.5 [24]	89.20	100.30	112.76	94.7 [20] 86 [26] 109.6 [27]	
$B^{'}$	3.82	3.65	3.565		4.02 [21] 3.58 [25] 3.85 [23]	3.94	3.826	3.749	3.852 [20] 3.70 [28]	

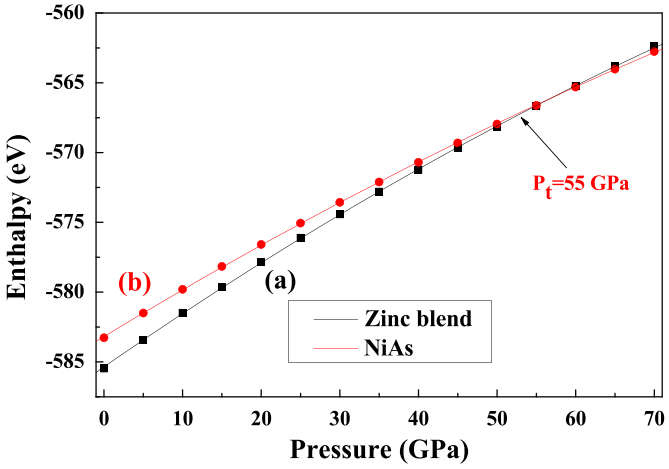

Fig. 3. The formation enthalpy as a function of pressure in zinc blend (a) and NiAs (b) structures for BeSe.

Table 2
Elastic constants C_{ij}, Debye temperature Θ_D, bulk modulus B, shear modulus G, Young's modulus E_H, Poisson's ratio σ_H, anisotropy factor A^U and ratio B_H/G_H for BeSe in zinc blend and NiAs structures.

		Zinc blend GGA	LDA	other	NiAs GGA	LDA
C_{11} (GPa)		120.06	137.22	117 [22] 145 [27]	140.27	167.04
C_{12} (GPa)		30.73	55.94	45.5 [29] 51 [27]	71.51	80.20
C_{44} (GPa)		66.2	74.35	73.39 [29] 61 [27]	8.48	14.57
C_{13} (GPa)					36.45	46.51
C_{33} (GPa)					178.40	202.79
Θ_D (K)		460.91	465.77	407 [29]	280.75	332.74
B(GPa)	B_V	60.51	83.08		83.08	98.15
	B_R	60.51	83.08		83.08	98.15
	B_H	60.51	83.08		83.08	98.14
G (GPa)	G_V	131.16	60.86	66.24 [30]	31.23	60.86
	G_R	127.51	55.83	61.14 [30]	16.22	55.83
	G_H	129.34	58.53	63.78 [30]	23.73	58.53
E_H (GPa)		129.34	141.82	153.42 [30]	65.00	86.89
σ_H		0.138	0.21	0.203 [30]	0.36	0.35
A^U		0.188	0.45		4.62	2.60
B_H/G_H		0.46	1.41	1.349 [30]	3.5	3.05

is in good agreement with that quoted in the literature 56 GPa [1].

3.2. Elastic constants

Elastic constants give information on binding between adjacent atomic planes, anisotropic character of bonds and elastically stability. Pressure is an important thermodynamic parameter in everyday life.

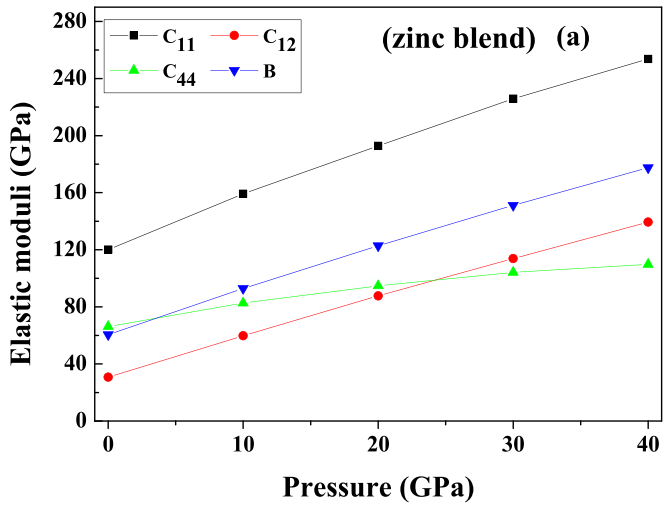

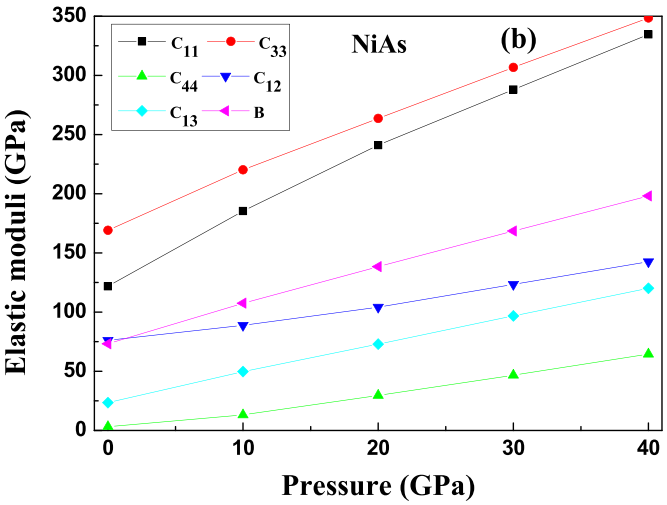

Fig. 4. Elastic moduli as a function of pressure for BeSe in zinc blend (a) and NiAs (b) structures.

Pressure measurement is a non-destructive test of metallurgical materials; and depends on the strength of the anvil material. The diamond has the highest Bulk Modulus ~440 GPa; among all known materials, so it is used as an anvil to achieve a very high pressure. Table 2 includes elastic moduli for beryllium selenide in both phases within GGA and LDA approaches. To date, no experiment elastic constants for NiAs phase are available to be compared with our results. Future experiment measurements will test our prediction calculation. Our elastic constants for

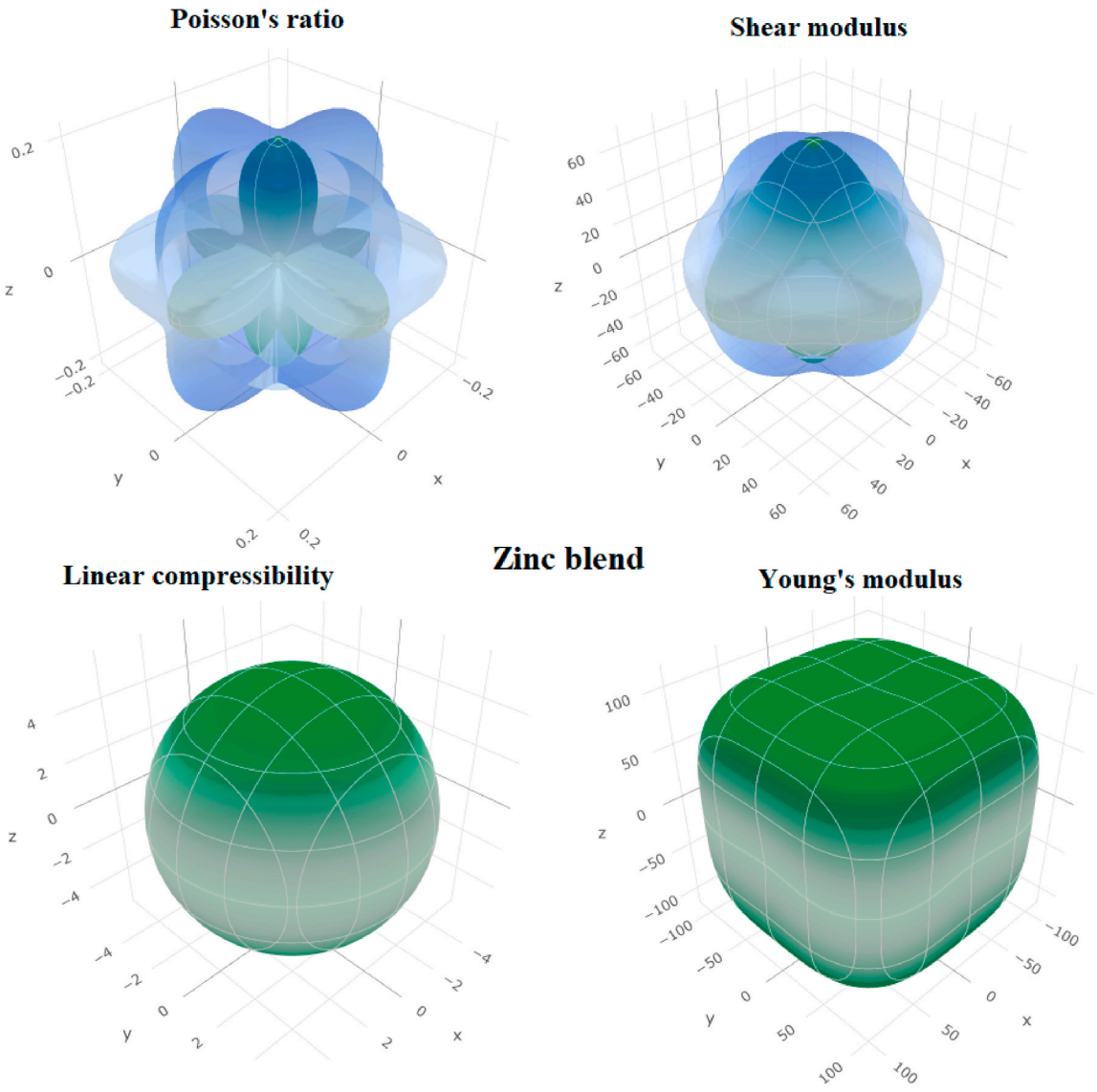

Fig. 5. The directional dependent on shear modulus, Young's modulus, linear compressibility and Poisson's ratio for BeSe in B3 structure.

Table 3
Directional dependent on Young's modulus E, linear compressibility β, shear modulus G and Poisson's ratio σ for BeSe in zinc blend and NiAs structures.

Parameters		Young's modulus E_{min} E_{max}		Linear compressibility β_{min} β_{max}		Shear modulus G_{min} G_{max}		Poisson's ratio σ_{min} σ_{max}	
Zinc blend	GGA	107.54	145.55	5.5083	5.5083	44.665	44.665	0.00989	0.25347
	LDA	104.83	171.79	4.0142	4.0142	40.644	74.354	0.00386	0.40923
NiAs	GGA	42.108	163.56	4.5012	4.5012	13.201	47.33	0.11861	0.62324
	LDA	49.954	185.29	3.3662	3.3662	14.575	64.941	0.10227	0.71926

Table 4
Sound velocities for BeSe along main directions in zinc blend and NiAs structures.

Material	Directions	[100]	[110]	[111]	[001]
Zinc blend	v_l (ms^{-1})	5439	5898	6043	–
	v_{t1} (ms^{-1})	3803	4305	3316	–
	v_{t2} (ms^{-1})	3803	3803	3316	–
NiAs	v_l (ms^{-1})	5192	–		6067
	v_{t1} (ms^{-1})	2187	–		1243
	v_{t2} (ms^{-1})	1243	–		1243

zinc blend structure are in good agreement with those cited in the literature performing within generalized gradient approximation [22,27,29,30]. The key criterion for mechanical stability of a crystal is that the strain energy must be positive [31]. Elastic stability is ensured by checking the following relationships [32,33]:

$$\text{Zinc blend} \quad 0\langle C_{11}+2C_{12}, 0\langle C_{44}, 0\langle C_{11}-C_{12}, C_{12}\langle B\langle C_{11} \tag{1}$$

$$\text{NiAs} \quad 0\langle C_{11}-|C_{12}|, 0\langle C_{33}(C_{11}+C_{12})-2C_{13}^2, 0\langle C_{44} \tag{2}$$

We note that our elastic constants verify the stability criteria listed above, therefore, beryllium selenide is stable in both structures at ambient temperature and equilibrium pressure. Fig. 4 shows the

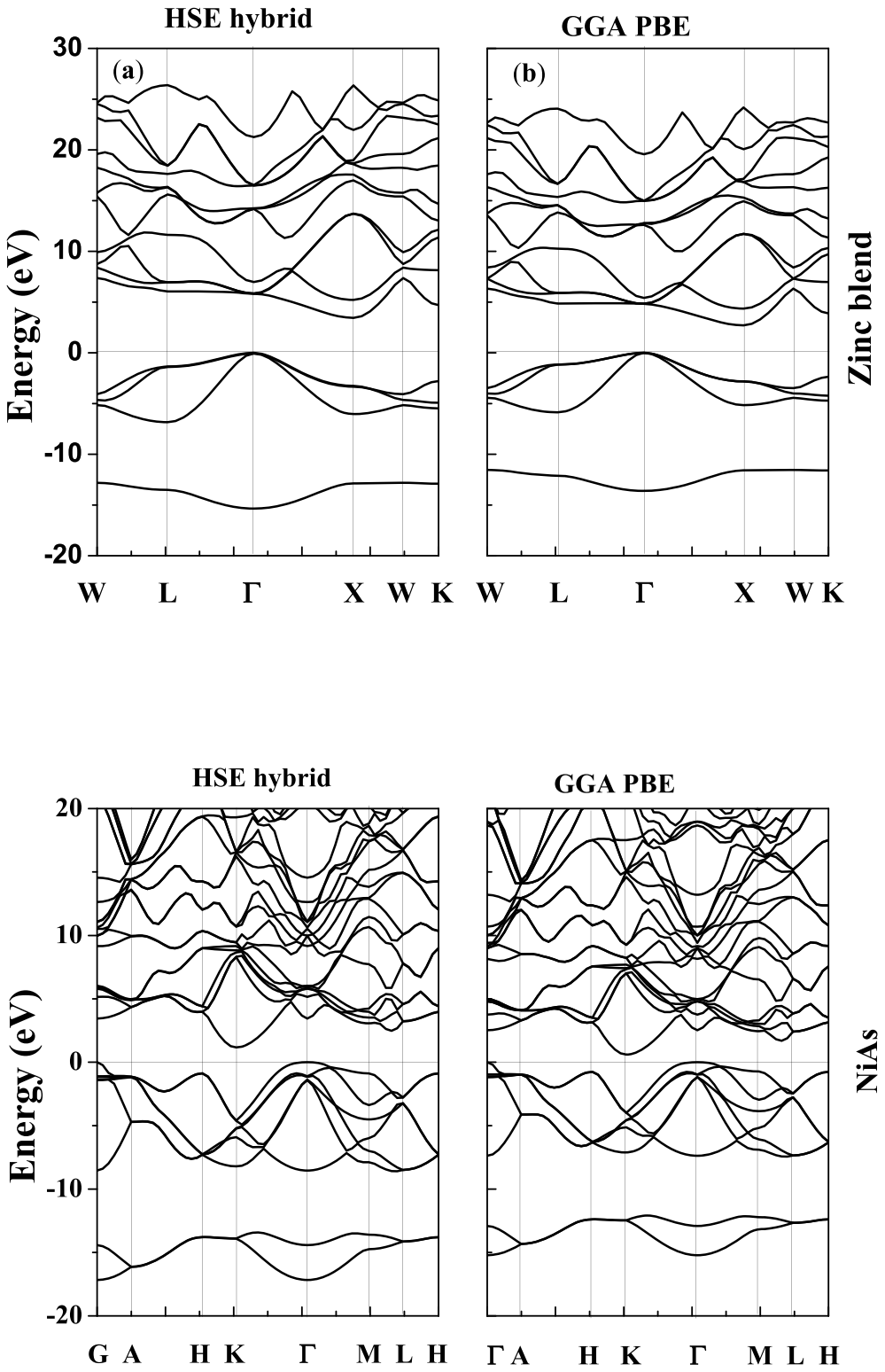

Fig. 6. Band structures for BeSe at various symmetry points into Brillouin zone in zinc blend (a) and (b) NiAs phases.

dependence of elastic moduli on pressure for beryllium selenide in zinc blend and NiAs phases. It was noted that all elastic moduli increase monotonously when the pressure is enhanced. The bulk modulus calculated from elastic constants is nearly the same as obtained from equation of state fitting. This is a sign of the exact calculation of our results. The bulk modulus B, shear modulus G, Young's modulus E_H, Poisson's ratio σ_H, anisotropy factor A^U and B_H/G_H ratio for BeSe calculated from elastic constants using Voigt [34], Reuss [35] and Hill [36] approximations are listed in Table 2. The Poisson's ratio for BeSe in both phases is removed from the limit value 0.25, so the bonding is covalent. The factor anisotropy value in both phases using GGA and LDA indicates that BeSe has a strong anisotropy. The reported B_H/G_H value translates that zinc blend phase is brittle, while NiAs is ductile. The anisotropic elastic factor gives information about the material properties in specific directions. Fig. 5 visualizes the directional dependent of shear modulus, Young's modulus, linear compressibility and Poisson's ratio in

Table 5
Band gaps for BeSe at equilibrium between various symmetry points in zinc blend and NiAs structures.

	Zinc blend GGA	LDA	HSE hybrid	Exp	other	NiAs GGA	LDA	HSE hybrid
$E_{\Gamma-\Gamma}$ (eV)	4.84	4.42	5.81	4.72 [3] 5.5 [43]		2.55	2.43	3.45
E_{L-L} (eV)	5.65	5.52	7.40			4.64	4.88	6.02
E_{X-X} (eV)	5.41	5.20	6.71					
$E_{\Gamma-X}$ (eV)	2.85	2.408	3.45	4–4.5 [3]	2.41 [41] 3.12 [19]			
$E_{\Gamma-L}$ (eV)	4.60	4.39	6.05		4.33 [21]	2.38	2.27	6.23
$E_{\Gamma-K}$ (eV)	3.94	3.62	4.71	4.73 [42]		0.68	0.51	1.16
E_{M-M} (eV)						3.28	2.98	3.94

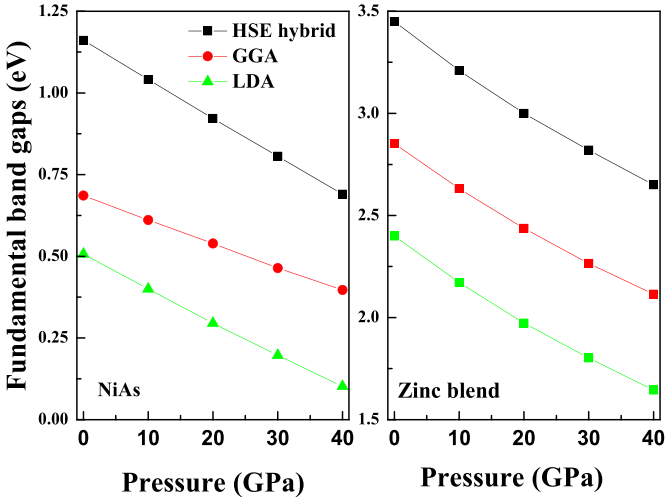

Fig. 7. Dependence on pressure of fundamental band gaps for BeSe in zinc blend (a) and NiAs (b) structures.

3D using ELATE software [37] for BeSe in zinc blend phase. The minimum and maximum of each parameter are visualized by green and blue colors. The shape is spherical for isotropic material and any distortion indicates anisotropy. Linear compressibility is isotropic, while Young's modulus, shear modulus and Poisson's ratio are anisotropic. The predicted maximum and minimum values of directional dependent of Young's modulus, linear compressibility, shear modulus and Poisson's ratio are listed in Table 3 in both phases within GGA and LDA.

3.3. Debye temperature

The Debye temperature depends on specific heat and melting temperature. The Debye temperature calculated from elastic constants is the same as that determined from specific heat measurements at low temperature. The formalism used in the calculation of Debye temperature and elastic wave velocities is in Refs. [38–40]. The GGA and LDA Debye temperature for both BeSe phases is reported in Table 2. LDA Debye temperature value is greater than that calculated by GGA. Our Debye temperature is in reasonable agreement with that quoted in the literature [29]. The predicted elastic wave velocities along [100], [110], [111] and [001] directions using GGA for both BeSe phases are listed in Table 4. Longitudinal waves are fastest according to [111] direction and shear waves are slowest along [001] direction.

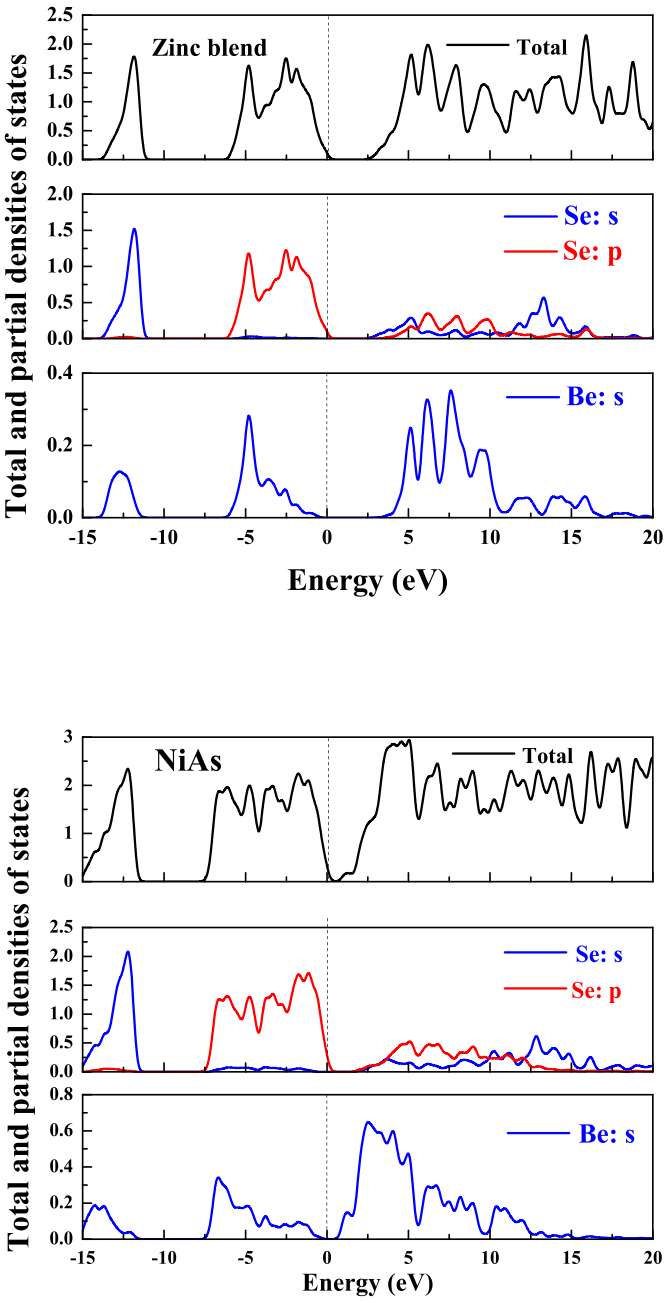

Fig. 8. Total and partial densities of states (TDOS) and (PDOS) for BeSe in zinc blend (a) and NiAs (b) structures.

3.4. Electronic properties

Fig. 6 shows the band structure for BeSe in both phases at various symmetry points in the Brillouin zone using GGA-PBE and HSE hybrid functional. It is noted that our results accurately give the indirect band gap Γ-X (Γ-K) in zinc blend (NiAs) structure and predict a semiconductor nature. Band gaps between various symmetry points in the Brillouin zone within HSE hybrid, GGA and LDA are reported in Table 5. Our band gaps for BeSe in zinc blend structure computed within GGA and LDA are in good agreement with other calculations [19,21,41]. The band gap in zinc blend structure calculated using GGA and LDA (HSE hybrid functional) is lower than (closer to) the experiment value located between 4 and 4.5 eV [3]. The HSE hybrid functional gives a fundamental gap closer to its experimental value. We can also see that the width of the valence band for BeSe in zinc blend structure consists of two zones

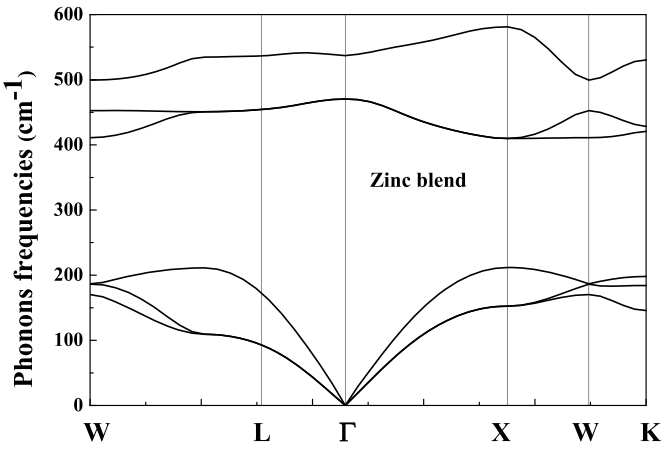

Fig. 9. Phonons dispersions curves for BeSe in Zinc blend structure.

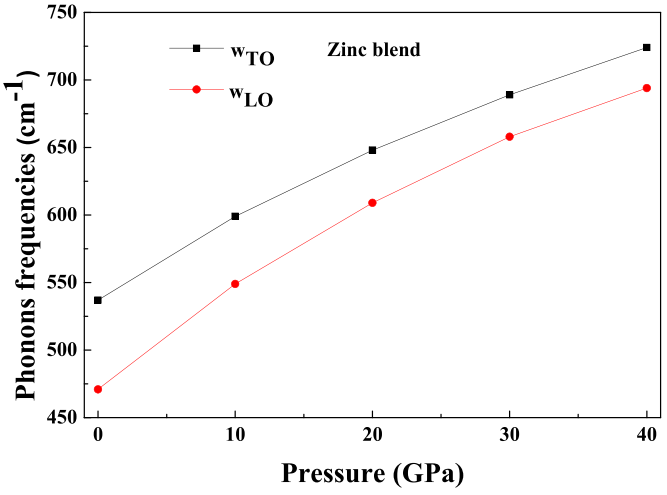

Fig. 10. Dependence on pressure of phonons frequencies for BeSe at Γ point in zinc blend structure.

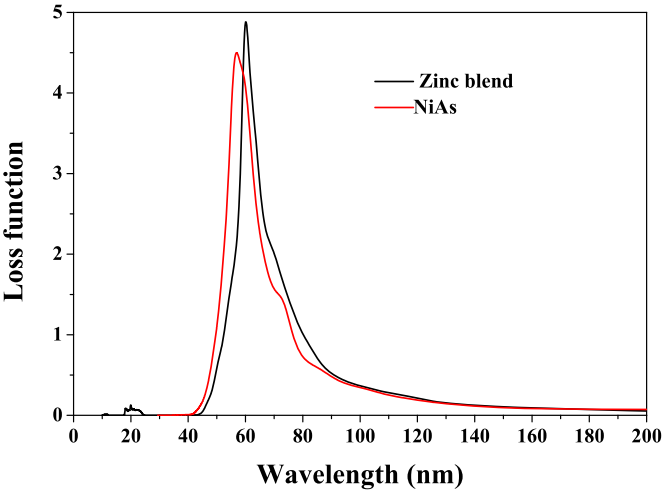

Fig. 11. The loss function versus wavelength for BeSe in zinc blend and NiAs structures.

separated by a gap 5.9773 eV and 5.6681 eV for HSE hybrid functional and GGA-PBE respectively. Fig. 7 displays the dependence of indirect fundamental band gap on pressure using GGA-PBE, LDA and HSE hybrid

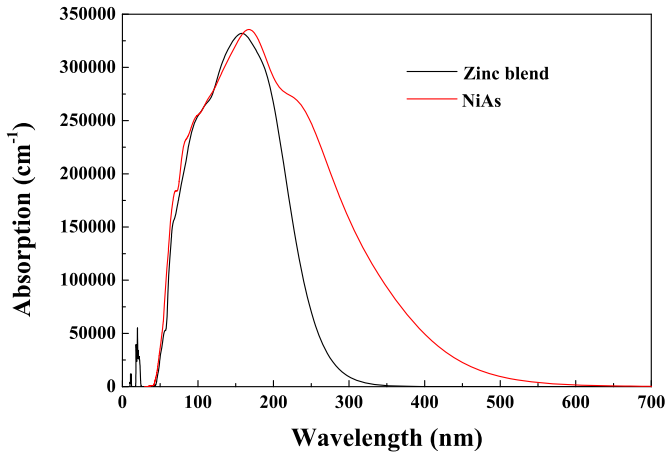

Fig. 12. The absorption as a function of the wavelength for BeSe in zinc blend and NiAs structures.

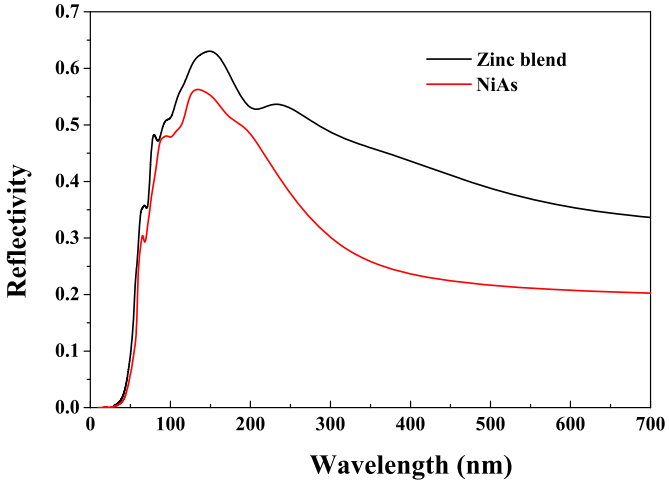

Fig. 13. The reflectivity as a function of wavelength for BeSe in zinc blend and NiAs structures.

functional for BeSe in zinc blend and NiAs phases. The fundamental indirect band gap decreases monotonously with increasing pressure in both structures. Our computed direct and indirect band gaps at equilibrium for zinc blend phase calculated using HSE hybrid functional are in good agreement with experiment [3,42,43]. Plots of total and partial densities of states TDOS and PDOS for BeSe at equilibrium lattice constant are shown in Fig. 8 in both structures. We distinguish two regions in the valence band. The lower valence band is located between −13.75 and −11.09 eV (−14.99 to −11.34 eV) and the upper valence band position is E_F to −6.06 eV (E_F to −7.55 eV) for zinc blend (NiAs) phase. It is shown that Se: p and Be: s orbital are response for the upper valence band. The first conduction band consisting of Be: s and Se: p orbital, with small contribution of Se: s site is wider for both structures. The optical transition occurs from Se: p state to Be: s site. There is hybridization between Se: p and Be: s in the upper valence band, which translates their covalent bonding.

3.5. Phonons frequencies

Fig. 9 shows phonons dispersions curves for BeSe in zinc blend structure at various symmetry points. Optical (acoustical) phonons exhibit two couplets of longitudinal optical (LO) {longitudinal acoustical (LA)} and transverse optical (TO) {transverse acoustical (TA)} modes and confirm the dynamical stability of BeSe in zinc blend phase.

Optical and acoustical phonons present the following characteristics:

(i) Longitudinal and transversal optical (acoustical) branches are separated by a frequency gap 16.06 cm^{-1} (198 cm^{-1}) in zinc blend structure.
(ii) The maximum of longitudinal optical phonons branches is located at X point in zinc blend structure.

Fig. 10 shows phonons frequencies ω_{LO} and ω_{TO} for BeSe at Γ point as a function of pressure in zinc blend structure. There is a monotonous increase in ω_{LO} and ω_{TO} when the pressure is enhanced. The values of ω_{LO} and ω_{TO} at Γ point at equilibrium are 537 cm^{-1} and 471 cm^{-1}.

3.6. Optical properties

3.6.1. Loss function

We plot in Fig. 11 the loss function spectra versus wavelength for BeSe in zinc blend and NiAs structures. There are high and low loss regions in the electronic loss function. The high loss region has wavelength range located between 42 and 90 nm. It starts after the ionization edge and translates the oxidation of Se: p state. The low loss function wavelength range is less than 40 nm and greater than 90 nm, which provides information about composition and electronic structure. The maximum loss function reaches the value 4.84 (4.49) at 60.32 nm (57.25 nm) in zinc blend (NiAs) structure. There is no loss in the ultra violet and visible light domain.

3.6.2. Optical absorption

The polycrystalline polarization method is used in the calculation of the optical absorption. This method includes a medium and isotropic electric field vector. We applied a smearing value of 0.1 to obtain more distinguishable absorbance peaks. The obtained absorption peaks as depicted in Fig. 12 are attributed to the photo transition energies from the maximum valence band to the minimum conduction band under ultra violet light irradiation. This material can absorb photons of ultra violet light (140–120 nm). The high absorption value is 330,142 (334,474) at wavelength of 163.6 nm (163 nm) for zinc blend (NiAs) phase. Indeed, to be a good candidate for photo catalysis in the ultra violet light domain (120–400 nm), a solid material must absorb maximum of ultra violet light 331,971 cm^{-1} (335,643 cm^{-1}) in zinc blend (NiAs) structure, shows narrow and indirect band gap and also have an appropriate position in energy of their valence and conduction bands. The maximum of absorption corresponds to the maximum of reflectivity and no loss function.

3.6.3. Optical reflectivity

The amount of light that is incident on the surface of photo catalytic material can be estimated from the reflectivity, which is related to the absorbance of that material. The reflectivity for BeSe as shown in Fig. 13 starts at 0.007 and corresponds to a wavelength around 33 nm. It reaches a maximum value 0.63 (0.56) at 149 nm (136.5 nm) in zinc blend (NiAs) structure. It is reported that the lower reflectivity indicates higher light absorption [44]. The reflectivity in the ultra violet light domain (120–400 nm) is 63% (56%) in zinc blend (NiAs) structure. While in the visible light (400–800 nm), it is 43% (23%) for zinc blend (NiAs) phase.

4. Conclusion

The beryllium selenide in zinc blend and NiAs phases was studied using PP-PW method based on density functional theory within GGA-PBE, LDA and HSE hybrid functional. Equilibrium lattice parameters in both phases are in good agreement with available experiment and theoretical data. Shear modulus, Young's modulus, Poisson's ratio, average sound velocities and Debye temperature are estimated using Voigt-Reuss-Hill approximations in zinc blend and NiAs phases. The absorption of maximum ultra violet light 331,971 cm^{-1} (335,643 cm^{-1}) in zinc blend (NiAs) structure, the narrow and indirect band gap and the appropriate position in energy of valence and conduction bands make BeSe as good candidate for photo catalysis. We performed transverse and longitudinal optical phonons frequencies ω_{TO} and ω_{LO} at Γ point in zinc blend phase for BeSe. BeSe in zinc blend phase shows an isotropic linear compressibility and anisotropic Young's modulus, shear modulus and Poisson's ratio. Elastic constants and bulk modulus follow practically the linear variation as a function of pressure. The high loss function translates the oxidation of Se: p state for BeSe in both phases. Longitudinal and transversal optical (acoustical) branches are separated by a frequency gap 16.06 cm^{-1} (198 cm^{-1}) in zinc blend structure. The reflectivity in the ultra violet light domain is 63% (56%) in zinc blend (NiAs) structure. While in the visible light, the reflectivity is 43% (23%) for zinc blend (NiAs) phase.

Credit author statement

Ghebouli Mohamed Amine: Conceptualization, Formal analysis, Funding acquisition; Ghebouli Brahim: Data curation; Chihi: Project administration, Resources, Software; Fatmi: Investigation, Methodology, Supervision, Validation, Visualization, Writing – original draft, Writing - review editing.

Declaration of competing interest

The authors declare that they have no known competing financial interests or personal relationships that could have appeared to influence the work reported in this paper.

References

[1] S. Dahbi, V. Mankad, P.K. Jha, J. Alloys Compd. 617 (2014) 905.
[2] M. González-Díaz, P. Rodríguez-Hernández, A. Munõz, Phys. Rev. B55 (1997) 14043.
[3] W. Yim, J. Dismukes, E. Stofko, R. Paff, J. Phys. Chem. Solid. 33 (1972) 501–505.
[4] G.P. Srivastava, H.M. Tütüncü, N. Günhan, Phys. Rev. B70 (2004) 85206.
[5] R. Khenata, A. Bouhemadou, M. Hichour, H. Baltache, D. Rached, M. Rérat, Solid State Electron. 50 (2006) 1382–1388.
[6] B. Bouhafs, H. Aourag, M. Ferhat, M. Certier, J. Phys. Condens. Matter 11 (1999) 5781.
[7] R. Pandey, S. Sivaraman, J. Phys. Chem. Solid. 52 (1991) 211.
[8] S. Asano, N. Yamashita, Y. Nakao, Phys. Status Solidi 89 (1978) 663.
[9] Y. Nakanishi, T. Ito, Y. Hatanaka, G. Shimaoka, Appl. Surf. Sci. 66 (1992) 515.
[10] M.D. Segall, P.J.D. Lindan, M.J. Probert, C.J. Pickard, P.J. Hasnip, S.J. Clark, M. C. Payne, J. Phys. Condens. Matter 14 (2002) 2717.
[11] P. Hohenberg, W. Kohn, Phys. Rev. B 136 (1964) 864.
[12] W. Kohn, L.J. Sham, Phys. Rev. A 140 (1965) 1133.
[13] D. Vanderbilt, Phys. Rev. B 41 (1990) 7892.
[14] H.J. Monkhorst, J.D. Pack, Phys. Rev. B 13 (1976) 5188.
[15] J.P. Perdew, K. Burke, M. Ernzerhof, Phys. Rev. Lett. 77 (1996) 3865.
[16] S. Goedecker, M. Teter, J. Hutter, Phys. Rev. B 54 (1996) 1703.
[17] T.H. Fischer, J. Almlof, J. Phys. Chem. 96 (1992) 9768.
[18] H. Luo, K. Ghandehari, R.G. Greene, A.L. Ruoff, Phys. Rev. B 52 (1995) 7058.
[19] G. Kalpana, G. Pari, A. Mookerjee, A.K. Bhattacharyya, Int. J. Mod. Phys. B 12 (1998) 1975.
[20] A. Munõz, P. Rodriguez-Hernandez, A. Mujica, Phys. Rev. B 54 (1996) 11861.
[21] C.M.I. Okoye, Eur. Phys. J. B 39 (2004) 5.
[22] D. Heciri, L. Beldi, S. Drablia, H. Meradji, N.E. Derradji, H. Belkhir, B. Bouhafs, Comput. Mater. Sci. 38 (2007) 609–617.
[23] K. Bouamama, K. Daoud, K. Kassali, Modelling Simul. Mater. Sci. Eng. 13 (2005) 1153.
[24] R. Dutta, S. Alptekin, N. Mandal, J. Phys. Condens. Matter 25 (2013) 125401.
[25] A.V. Postnikov, O. Pages, T. Tite, M. Ajjoun, J. Hugel, Phase Transitions 78 (2005) 219.
[26] N. Munjal, V. Sharma, G. Sharma, V. Vyas, B.K. Sharma, J.E. Lowther, Phys. Scripta 84 (2011), 035704.
[27] A. Berghout, A. Zaoui, J. Hugel, J. Phys. Condens. Matter (2006) 10365.
[28] F.E.H. Hassan, H. Akbarzadeh, Comput. Mater. Sci. 35 (2006) 423.
[29] Fanjie Kong, Gang Jiang, Physica B 404 (2009) 3935–3940.
[30] Surya Chattopadhyaya, Utpal Sarkar, Bimal Debnath, Manish Debbarma, Debankita Ghosh, Sayantika Chanda, Rahul Bhattacharjee, Phys. B Condens. Matter 563 (2019) 1–22.
[31] J.F. Nye, Physical Properties of Crystals, Oxford University Press, Oxford), 1985.
[32] W.D.L. Cruz, J.A. Duaz, L. Mancera, N. Takeuchi, G. Soto, J. Phys. Chem. Solid. 64 (2003) 2273.
[33] M. Born, K. Hang, Dynamical Theory and Experiments I, Springer Verlag Publishers, Berlin, 1982.

[34] W. Voigt, Lehrbuch der Kristallphysik, Teubner, Leipzig, 1928.
[35] A. Reuss, Z. Angew, Math. Mech. 9 (1929) 49–58.
[36] R. Hill, Proc. Phys. Soc., London 65 (1952) 349.
[37] M. Mattesini, M. Magnuson, F. Tasnádi, C. Höglund, Igor A. Abrikosov, L. Hultman, Phys. Rev. B 79 (2009) 125122.
[38] O.L. Anderson, J. Phys. Chem. Solid. 24 (1963) 909.
[39] E. Schreiber, O.L. Anderson, N. Soga, Elastic Constants and Their Measurements, McGraw-Hill, New York), 1973.
[40] B.B. Karki, L. Stixrude, S.J. Clark, M.C. Warren, G.J. Ackland, J. Crain, Am. Miner. 82 (1977) 51.
[41] D. Rached, M. Rabah, N. Benkhettou, R. Khenata, B. Soudini, Y. Al-Douri, H. Baltache, Comput. Mater. Sci. 37 (2006) 292–299.
[42] R.L. Sarkar, S. Chatterjee, J. Phys. C Solid State Phys. 10 (1) (1977) 57–62, https://doi.org/10.1088/0022-3719/10/1/011.
[43] K. Wilmers, T. Wethkamp, N. Essar, C. Cobet, F. Richter, V. Wagner, H. Lugauer, F. Fischer, T. Gerhard, M. Keim, Phys. Rev. B 59 (1999) 10071–10075.
[44] P.H. Berning, G. Hass, R.P. Madden, J. Opt. Soc. Am. 50 (6) (1960) 586–597. JOSA.